

Real-Time EMT Modeling and Coordinated Frequency Control of GW-Level Offshore Wind-Hydrogen Energy System[#]

Chunjun Huang¹, José Luis Rueda Torres^{1*}

¹ Department of Electrical Sustainable Energy, Delft University of Technology

(Corresponding Author: J.L.RuedaTorres@tudelft.nl)

ABSTRACT

Integrating gigawatt-scale offshore wind-hydrogen energy systems (OWHESs) is pivotal for the energy transition, yet their dynamic interactions and grid-support capabilities remain insufficiently explored. This paper addresses this gap by developing a real-time electromagnetic transient model of a 2 GW OWHES, which is implemented on a commercial real-time digital simulator (RTDS). Furthermore, a novel communication-free coordinated frequency control strategy is proposed, which synergistically harnesses the flexibility of the HVDC system, wind power plants, and electrolyzer plants. Real-time simulation results demonstrate the model's ability to capture the OWHES dynamics. Moreover, results from a significant generation loss scenario demonstrate the proposed control's superiority over existing methods, as it markedly improves the onshore frequency nadir and reduces the rate of change of frequency. This confirms its effectiveness in enhancing onshore frequency stability and showcases the potential of OWHESs as a valuable source of grid ancillary services.

Keywords: real-time digital simulation, power-to-hydrogen plant, HVDC transmission, offshore wind power plant

1. INTRODUCTION

The rapid growth of offshore wind power has made it a cornerstone of clean energy transition, with countries such as the Netherlands setting ambitious targets of 70 GW capacity by 2050 [1]. To fully utilize this renewable resource, hydrogen production is increasingly adopted to as a complementary pathway, providing large-scale energy storage, operation flexibility, and cross-sectoral integration [2,3]. Integrating offshore wind power with electrolyzers into offshore wind-hydrogen energy systems (OWHESs) offers a promising route for both electricity supply and green hydrogen production.

Despite this potential, operating gigawatt-scale OWHESs presents significant challenges. Wind variability, grid disturbances, and uncertain hydrogen demand introduce complex dynamic interactions that threaten system stability. Existing studies have mainly analyzed offshore wind generation or hydrogen production separately, leaving the real-time dynamic behavior of integrated OWHESs insufficiently explored. Suitable electromagnetic transient (EMT) modeling is required to capture the fast dynamics of wind power plants, high-voltage direct current (HVDC) transmission, and electrolyzers, and to evaluate OWHES dynamics.

This paper addresses these gaps by developing a real-time EMT model of a 2 GW OWHES, implementing it on the commercial real-time digital simulator (RTDS). Moreover, a coordinated frequency control strategy is proposed to harness the flexibility of electrolyzers, wind power plants, and HVDC for supporting onshore frequency stability. Real-time simulation demonstrates the effectiveness of the proposed modeling and control methods, providing new insights into the real-time and reliable operation of GW-level OWHESs.

2. PROPOSED MODELING APPROACH OF 2 GW OFFSHORE WIND-HYDROGEN ENERGY SYSTEM

The topology of the developed 2 GW OWHES is illustrated in Fig. 1. This system comprises three wind power plants (WPPs): one with a 1.5 GW capacity and two rated at 500 MW each, as well as two 250 MW electrolyzer plants (ELPs). A bipolar MMC-based HVDC transmission system links the OWHES to a 400 kV onshore bus, enabling electrical energy exchange between offshore and onshore.

2.1 Electrolyzer unit

The ELP is represented as an aggregated large-scale unit by equivalently scaling multiple 1 MW electrolyzer modules and neglecting intra-module dynamics. Each

[#] This is a paper for the 17th International Conference on Applied Energy (ICAE2025), December 8-12, 2025, Bangkok, Thailand.

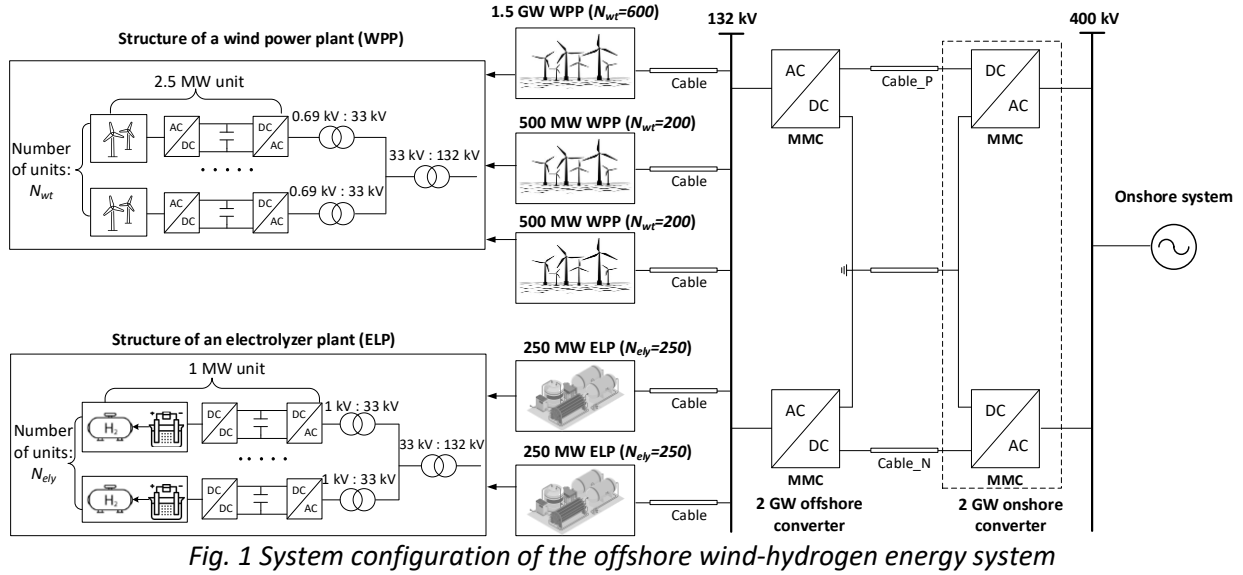


Fig. 1 System configuration of the offshore wind-hydrogen energy system

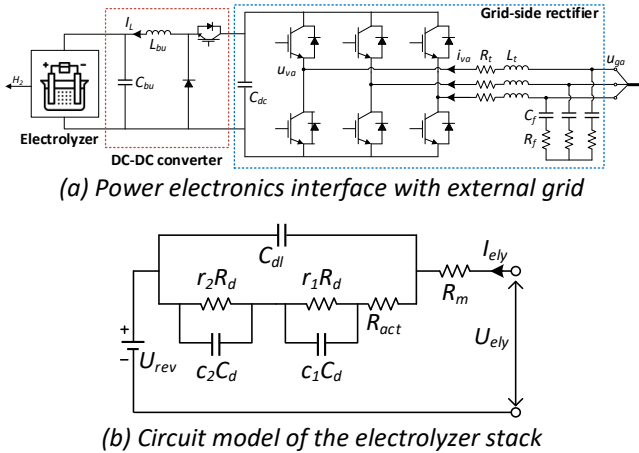


Fig. 2 System configuration of the electrolyzer unit

module consists of an electrolyzer stack, a DC-DC converter, a grid-side rectifier, as illustrated in Fig. 2(a). The DC-DC converter operates as a buck converter supplying the required DC current to the electrolyzer, while the rectifier connects to the external AC system.

Electrolyzer electrical behavior is governed by the nonlinear polarization curve, where the applied voltage must overcome the reversible voltage and the associated overpotentials [4]. For power system studies, this characteristic is approximated by the equivalent circuit shown in Fig. 2(b) [5]. Based on the circuit, the electrolyzer dynamics can be described as:

$$U_{ely}(s) = U_{rev} + I_{ely}(s)Z_{ely}(s) \quad (1)$$

$$Z_{ely}(s) = R_m + \frac{R_{act} + \frac{r_1 R_d}{r_1 R_d c_1 C_d s + 1} + \frac{r_2 R_d}{r_2 R_d c_2 C_d s + 1}}{\left(R_{act} + \frac{r_1 R_d}{r_1 R_d c_1 C_d s + 1} + \frac{r_2 R_d}{r_2 R_d c_2 C_d s + 1} \right) C_{dl} s + 1} \quad (2)$$

where R_i , C_i , r_i , c_i are the fitted parameters representing the main electrochemical effects, can be fitted through experimental testing of electrolyzers [5].

The hydrogen production rate is calculated using Faraday's law as:

$$\dot{n}_{H_2} = \frac{\eta_F N_{cell} I_{stack}}{zF} \quad (3)$$

where $z=2$ is the number of electrons transferred, F is the Faraday constant, 96485 C/mol; η_F is the Faradaic efficiency, approximately 1; N_{cell} is the number of cells.

The electrolyzer is interfaced through a two-stage converter comprising a buck-type DC-DC converter and a three-phase voltage-source rectifier. The buck converter controls stack power for fast reference tracking (as shown in Fig. 3). A current reference is derived from the power reference and constrained by magnitude and rate limiters to obey feasible operating ranges and dynamic limits of the electrolyzer. The current controller then tracks this reference and generates the duty ratio D . This control structure enables partial-load operation and fast power response.

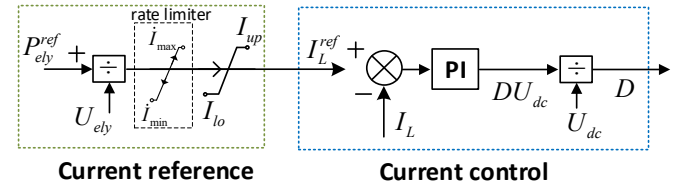


Fig. 3 Control structure of the buck converter

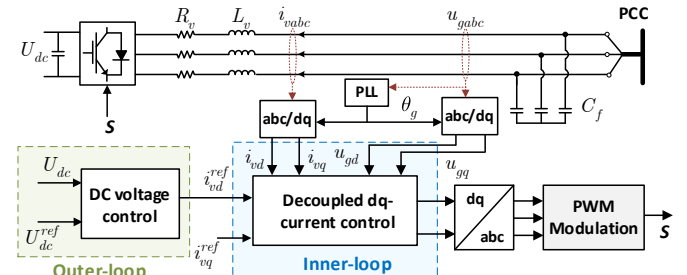


Fig. 4 Control structure of the grid-side rectifier

The grid-side rectifier adopts the standard dual-loop control shown in Fig. 4. The outer loop regulates DC-link voltage (d-axis), where reactive power (q-axis) is adjusted via directly setting the reactive current; while the inner dq current loop ensures decoupled current tracking. The resulting voltage reference is modulated via pulse-width modulation (PWM) to generate gating signals. This widely used architecture provides stable DC-link dynamics and grid-following characteristics.

2.2 Wind generator unit

The wind generator unit is modeled using the widely used Type-IV configuration, while the detailed modeling method and converter control are well established in the literature [6], as shown in Fig. 5. The wind turbine is coupled with a permanent magnet synchronous generator (PMSG), whose output is interfaced to external AC systems through a back-to-back two-level voltage source converter comprising the machine-side converter (MSC) and the grid-side converter (GSC).

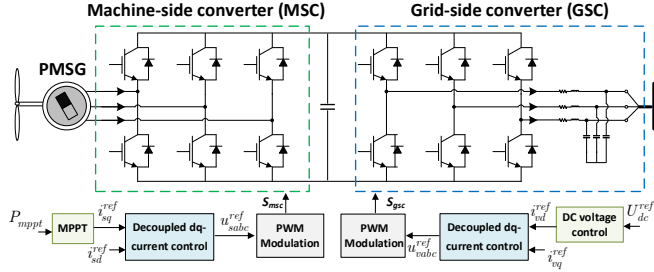


Fig. 5 System structure of the wind generator unit

The MSC, directly connected to the PMSG, works as a rectifier while regulating generator torque to enable maximum power point tracking (MPPT). Its control structure typically combines an outer-loop torque or power controller with an inner-loop current controller, and produces modulation signals for PWM switching. The GSC, in turn, works as an inverter, ensuring a stable DC-link voltage and regulating reactive power exchange with external systems. Its control system (shown in Fig. 5) adopts a hierarchical structure with outer-loop DC voltage regulation and inner-loop current control.

2.3 HVDC transmission system

As shown in Fig. 1, the OWHES is connected to onshore systems through a bipolar HVDC transmission system, which employs the widely used half-bridge modular multilevel converter (MMC) technology. The detailed modeling can be found in [7]. The control structure of the HVDC is shown in Fig. 6. Positive and negative poles are controlled symmetrically to maintain

balanced DC voltages and power flow. Different strategies are applied at the two terminals:

- 1) Onshore converter (Controller I) operates in grid-following mode, regulating the DC-link voltage and reactive power exchange with the onshore system;
- 2) Offshore converter (Controller II) operates in grid-forming mode, providing voltage and frequency references for the offshore system and acting as the slack bus to maintain offshore voltage and frequency.

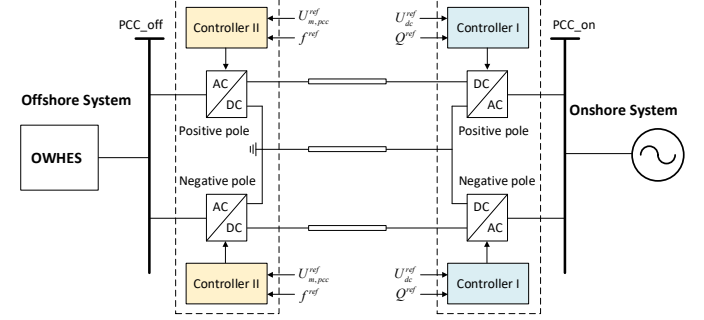


Fig. 6 Control structure of bipolar HVDC system

3. PROPOSED COORDINATED FREQUENCY CONTROL

Onshore contingencies (e.g., generator trips) cause active power imbalances and critical frequency deviations. Although OWHES can provide support, the HVDC link decouples offshore from onshore frequency dynamics. The state-of-the-art solution is communication-free frequency control (CFFC), which avoids latency and cost issues of communication-based methods [8]. However, how to design transient frequency control for OWHES within the CFFC framework to ensure fast frequency response and automatic recovery remains underexplored.

To address this, a CFFC-based coordinated frequency control is proposed, as illustrated in Fig. 7. The key idea is to use DC voltage as the intrinsic carrier of frequency information, enabling offshore units to sense onshore frequency deviations without communication. The operating principle is as follows:

- (1) **Step 1:** The onshore converter station adjusts its DC voltage $\Delta U_{dc,on}$ according to onshore frequency deviation Δf_{on} via control law $G_{hvdc1}(s)$ of the HVDC's fast frequency controller (FFC).
- (2) **Step 2:** Through HVDC dynamics, the offshore DC voltage $\Delta U_{dc,off}$ changes accordingly, which is mapped into an offshore frequency deviation Δf_{off} by control law $G_{hvdc2}(s)$ of the HVDC's FFC.
- (3) **Step 3:** ELPs and WPPs detect Δf_{off} and autonomously adjust active power based on their individual FFCs, contributing to onshore frequency stabilization.

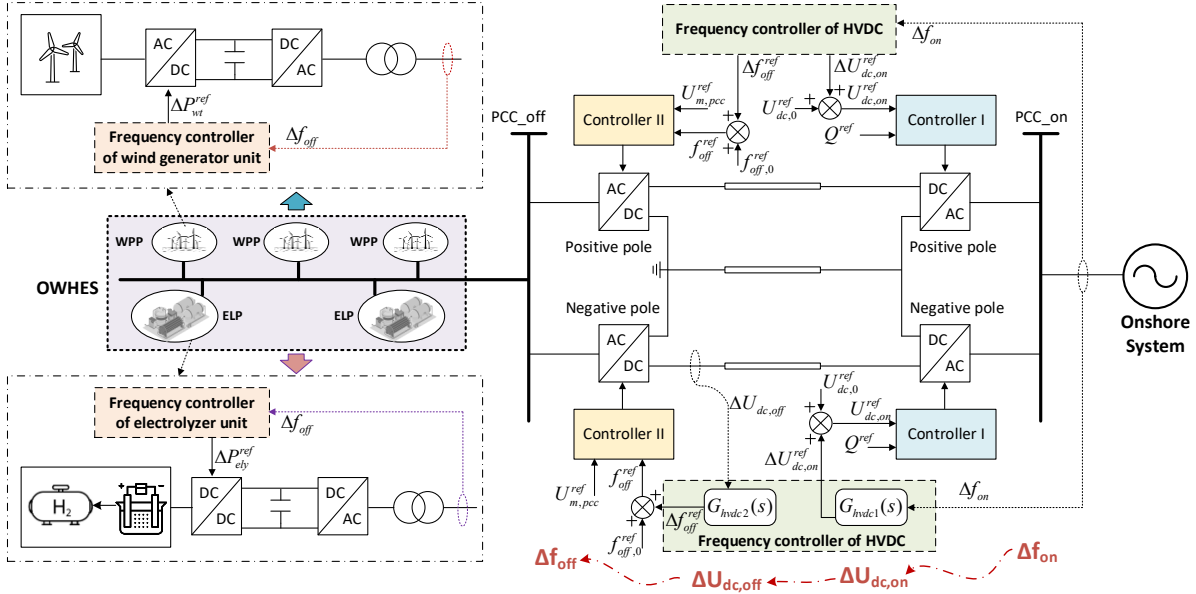


Fig. 7 Overall control framework of the proposed coordinated frequency control

3.1 Fast frequency controller of HVDC

As shown in Fig. 7, the HVDC FFC employs two transfer functions, respectively representing control action for the onshore and offshore converter, which can be described as:

$$G_{hvdcl}(s) = \frac{\Delta U_{dc,on}^{ref}(s)}{\Delta f_{on}(s)} = K_1 \frac{sT_h}{1 + sT_h} \quad (4)$$

$$G_{hvdcl2}(s) = \frac{\Delta f_{off}^{ref}(s)}{\Delta U_{dc,off}(s)} = \frac{K_2(U_{dc,off}(s) - U_{dc,0} - \Delta U_{dc,l})}{\Delta U_{dc,off}(s)} \quad (5)$$

where K_1 and K_2 are proportional gains; T_h is the washout filter constant; $U_{dc,0}$ is the nominal DC voltage; $\Delta U_{dc,l}$ is the voltage loss across the HVDC cable.

When controllers operate correctly, actual and reference values align, leading to:

$$\Delta f_{off}(s) = K_2 K_1 \frac{sT_h}{1 + sT_h} \Delta f_{on}(s) \quad (6)$$

This ensures that the offshore frequency deviation follows the onshore deviation and automatically returns to zero through the washout filter, guaranteeing system restoration after transients.

3.2 Fast frequency controller of electrolyzer plants

Fig. 8 depicts the detailed structure of the fast frequency controller for each electrolyzer unit. A combined inertia-droop control block generates an active power adjustment ΔP_{ely}^{ref} in response to both the rate of change of frequency (RoCoF) and frequency deviation, which is expressed by:

$$\Delta P_{ely}^{ref} = K_{d,ely} \Delta f_{off} + K_{i,ely} \frac{df_{off}}{dt} \quad (7)$$

where $K_{d,ely}$ and $K_{i,ely}$ are the droop and synthetic inertia parameters, respectively.

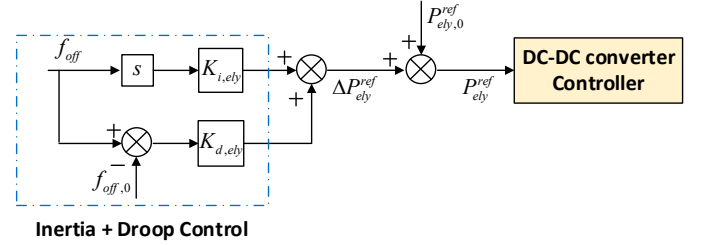


Fig. 8 Fast frequency controller for the electrolyzer unit

The final active power reference for the electrolyzer's DC-DC converter is then calculated by adding ΔP_{ely}^{ref} to the nominal reference $P_{ely,0}^{ref}$. This reference is implemented by the DC-DC converter controller as shown in Fig. 3, thereby regulating the electrolyzer's power consumption to provide frequency regulation.

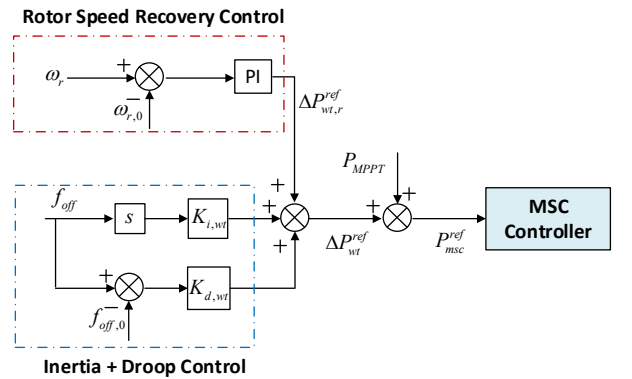


Fig. 9 Fast frequency controller for the wind generator

3.3 Fast frequency controller of wind power plants

The WPP's FFC is shown in Fig. 9. The proportional-derivative controller is used to form a synthetic inertia and droop control block. The block produces an active power reference as a function of the RoCoF and frequency deviation. By further incorporating a term derived from the rotor speed recovery control, the active power adjustment is obtained and expressed as:

$$\Delta P_{wt}^{ref} = K_{d,wt} \Delta f_{off} + K_{i,wt} \frac{df_{off}}{dt} + \underbrace{K_{p,r}(\omega_r - \omega_{r,0}) + K_{i,r} \int (\omega_r - \omega_{r,0}) dt}_{\Delta P_{wt,r}^{ref}} \quad (8)$$

where $K_{d,wt}$ and $K_{i,wt}$ are the droop and synthetic inertia parameters; $K_{p,r}$ and $K_{i,r}$ are the PI parameters of the rotor speed recovery control; $\omega_{r,0}$ represents the nominal rotor speed where the MPPT is achieved.

This active power adjustment ΔP_{wt}^{ref} is added to the nominal reference i.e. MPPT power P_{MPPT} , forming the final reference for the MSC of the wind generator. The MSC controller implements this reference, adjusting the wind generator's output active power to provide frequency regulation.

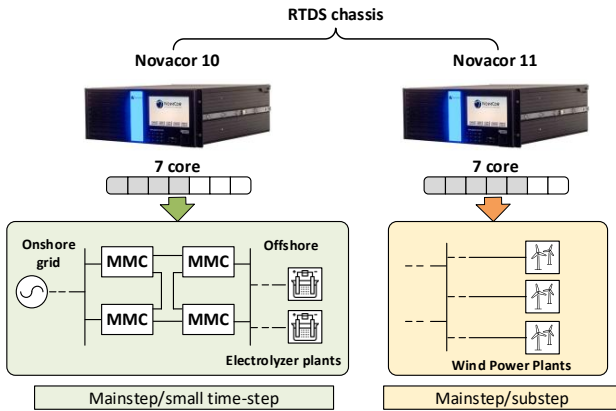


Fig. 10 Schematic of RTDS chassis allocation for implementing digital model of the OWHES

4. CASE STUDY

4.1 RTDS implementation

The proposed OWHES, depicted in Fig. 1, is implemented in the commercial RTDS platform to resolve EMT-level dynamics. Within RSCAD, the model is partitioned into two subsystems, which are executed on separate RTDS chassis, as configured in Fig. 10. For instance, chassis 10 simulates the onshore grid, HVDC link, electrolyzer plants, and their interconnection, using both the main-step (60 μ s) and small-step (2.8 μ s) environments, requiring four cores. Chassis 11 models all offshore wind power plants and their network, using the main-step and sub-step (3 μ s) environments, with five

cores assigned. This allocation enables efficient parallel execution of the large-scale OWHES.

4.2 Results and discussion

The proposed frequency control method is tested under an 80 MW generator trip in the onshore system at $t=2$ s. Furthermore, the proposed control is compared against existing frequency control strategies, as follows:

- **Without FFC:** No fast frequency control is applied
- **FFC from HVDC:** traditional CFFC-based frequency control of the HVDC system
- **FFC from HVDC and WPP:** traditional frequency control of HVDC-connected offshore WPPs [8].
- **Proposed control:** The proposed frequency control.

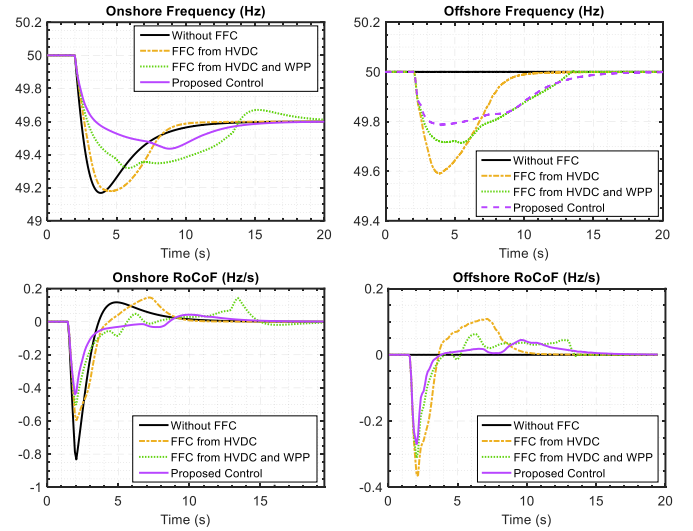


Fig. 11 System frequency response under various frequency control strategies

The frequency responses in offshore and onshore systems are shown in Fig. 11. The proposed control achieves the highest nadir (i.e. the maximum frequency deviation point) and lowest RoCoF of the onshore frequency among all control strategies, clearly outperforming existing methods. This benefit mainly arises from the electrolyzer plants, which provide additional, fast controllable power demand reduction. Furthermore, the washout filter in the proposed controller ensures that the offshore frequency returns to the nominal 50 Hz in steady state, preventing prolonged frequency support that could otherwise disrupt normal operation. Without this mechanism, extended frequency support could lead to inefficiencies such as reduced wind power generation and lower hydrogen production.

More details of the OWHES dynamic response with the proposed control are presented in Fig. 12. Following the frequency disturbance at $t=2$ s, the active power

transfer through the HVDC link rises sharply, providing immediate frequency support to the onshore system. This response is the result of three coordinated actions: 1) the HVDC FFC releases stored DC-link energy by temporarily lowering the DC voltage, which boosts power delivery to onshore; 2) the ELP FFC decreases electrolyzer load, releasing more active power for system support; 3) the WPP FFC extracts kinetic energy from turbine rotors, momentarily increasing output at the expense of a slight rotor speed reduction. These mechanisms jointly enhance the system's fast frequency response. After the transient support, all system variables including DC voltage, electrolyzer load, and rotor speed gradually return to their nominal values, demonstrating the system's self-restoration capability.

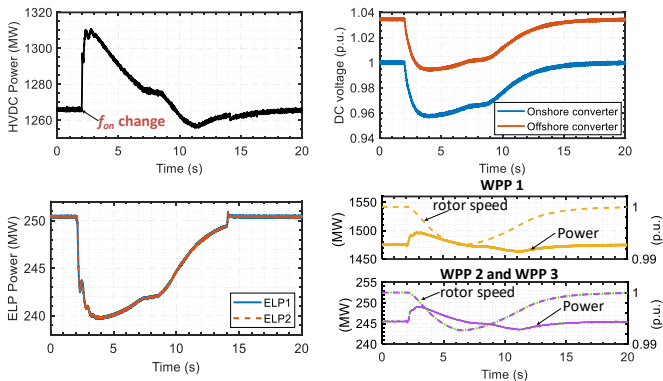


Fig. 12 OWHES response when using the proposed control

Overall, the results confirm that the proposed control enables OWHES to provide effective fast frequency regulation by coordinating HVDC, WPPs, and ELPs. Compared with existing approaches, it achieves higher frequency nadir and lower RoCoF, thereby improving frequency stability more effectively. Moreover, the built-in washout filter ensures that frequency support is temporary, preventing long-lasting deviations and avoiding efficiency losses such as reduced wind generation or hydrogen production.

5. CONCLUSIONS

This paper develops a real-time EMT model of a GW-scale OWHES based on the commercial RTDS platform, and further proposes a coordinated fast frequency control strategy. Building on the conventional CFFC framework, the approach effectively harnesses the synergistic capabilities of HVDC links, WPPs, and ELPs to deliver rapid and reliable frequency support. Real-time simulations demonstrate that the proposed control significantly improves the frequency nadir and RoCoF under a generation loss scenario, outperforming existing methods. Importantly, the system autonomously returns to nominal operation after events, ensuring frequency

stability without compromising long-term wind generation or hydrogen production.

These findings highlight the potential of OWHES to evolve from passive renewable integration assets into active stabilizing resources for future onshore systems with high renewable penetration. Future work will focus on refining the coordination mechanism through joint optimization of HVDC, WPP, and ELP frequency responses, thereby further improving the frequency support capability.

ACKNOWLEDGEMENT

The research work has received funding from TenneT TSO B.V. within the research project on “Adaptive fast active power control for stabilization of multiconverter dynamics in offshore electrical energy-hydrogen hubs - FUTURE SYSTEM”. It reflects only the authors' views, and the aforesaid organization is not responsible for any use that may be made of the paper's content.

REFERENCE

- [1] Ministerie van Economische Zaken en Klimaat. Kamerbrief windenergie op zee 2030-2050. <https://www.rijksoverheid.nl/documenten/kamerstukken/2022/09/16/kamerbrief-windenergie-op-zee-2030-2050#:~:text=Minister Jetten>.
- [2] North Sea Wind Power Hub. NSWPH Discussion paper on Grid-integrated offshore Power-to-Gas 2022. <https://northseawindpowerhub.eu/knowledge>
- [3] North Sea Wind Power Hub. Offshore Energy Hubs: Blueprints with Offshore Electrolysis 2024. <https://northseawindpowerhub.eu/knowledge>.
- [4] Olivier P, Bourasseau C, Bouamama PB. Low-temperature electrolysis system modelling: A review. *Renew Sustain Energy Rev* 2017;78:280–300.
- [5] Martinson CA, Van Schoor G, et al. Characterisation of a PEM electrolyser using the current interrupt method. *Int J Hydrogen Energy* 2014;39:20865–20878.
- [6] Honrubia-Escribano A, Gómez-Lázaro E, Fortmann J, Sørensen P, Martin-Martinez S. Generic dynamic wind turbine models for power system stability analysis: A comprehensive review. *Renew Sustain Energy Rev* 2018;81:1939–1952.
- [7] Guan M, Xu Z. Modeling and control of a modular multilevel converter-based HVDC system under unbalanced grid conditions. *IEEE Trans Power Electron* 2012;27:4858–4867.
- [8] Lin CH, Wu YK. Overview of Frequency-Control Technologies for a VSC-HVDC-Integrated Wind Farm. *IEEE Access* 2021;9:112893–921.